The CCD instrument background of the SMILE SXI

M. W. J. Hubbard[1], O. Hetherington[1], D. J. Hall[1], T. W. Buggey[1], S. Parsons[1], T. Arnold[1], A. Holland[1], C. Pagani[2], S. Sembay[2]

[1]Centre for Electronic Imaging, The Open University, Milton Keynes, MK7 6AA, U.K.
[2]X-ray and Observational Astronomy Group, Department of Physics & Astronomy, University of Leicester, LE1 7RH, UK

Key Points:

- SMILE will have two different instrument particle background rates depending on the radiation shutter door position being open or closed
- Closed background will be highest near solar maxima whilst open background is highest during solar minima
- Unfocussed instrument background is dominated by galactic cosmic ray protons.

Corresponding author: Michael Hubbard, michael.hubbard@open.ac.uk

Abstract
The ESA and CAS SMILE mission orbit is highly elliptical and will pass through multiple radiation environments. The Soft X-ray Imager (SXI) instrument aboard has a radiation shutter door designed to close when the surrounding radiation flux is high. The shutter door will close when passing below an altitude threshold to protect against trapped particles in the Earth's Van Allen Belts. Therefore, two radiation environments can be approximated based on the shutter door position: open and closed.

The instrument background for the CCDs that form the focal plane array of the SXI were evaluated for the two environments. Due to the correlation of the space environment with the solar cycle, the solar minima and maxima, the background was also evaluated at these two extremes. The results demonstrated that the highest instrument background will occur during solar minima due to the main contributing source being Galactic Cosmic Rays (GCRs). It was also found that the open background was highest for solar minima and that the closed background was highest during solar maxima. This is due to the radiation shutter door acting as a scattering centre and the changes in the energy flux distribution of the GCRs between the two solar extremes.

1 Introduction

The Soft X-ray Imager (SXI) (Sembay et al., 2016) instrument is one of the primary instruments aboard the Solar wind Magnetosphere Ionosphere Link Explorer (SMILE) spacecraft. The SMILE mission is designed to study how the solar wind impacts the Earth's magnetosphere and is led by a cooperation between the European Space Agency (ESA) and the Chinese Academy of Sciences (CAS) (Raab et al., 2016). The spacecraft includes an instrumentation suite comprising of the Soft X-ray Imager (SXI), the Ultra-Violet Imager (UVI), a Light Ion Analyser (LIA) and a MAGnetometer (MAG). The results from each instrument will be combined to provide a unique perspective of how the Earth's magnetosphere and ionosphere are impacted by the solar wind. The Northern hemisphere's aurora will be analysed in the ultra-violet band, whilst simultaneously, observations of the interaction between the Earth's dayside magnetosheath and the solar wind will be monitored in the soft X-ray band.

The SXI will observe the soft X-rays generated from the interaction between the solar wind and Earth's dayside magnetosheath. To achieve this SMILE will have a highly elliptical orbit and traverse multiple radiation environments. Each environment requires different shielding requirements due to their flux, energy spectra, particle composition and correlation with the solar cycle. These sources all impact the instrument background of X-ray telescope missions (Fioretti et al., 2012). The SMILE SXI is equipped with an active radiation shielding door and will close at low altitudes to protect against the Earth's trapped particle environments. Therefore, observation is limited to only a portion of the orbital path reducing the number of radiation environment sources present.

The SXI instrument includes Silicon Micro-Pore Optics (MPOs) in a lobster-eye configuration, which focuses X-rays towards the focal plane array (FPA). The FPA for the SMILE SXI contains two large area, back illuminated, Charge-Coupled Devices (CCDs), each with an area of approximately 8 cm×8 cm (Soman et al., 2018). A large detector design was compared to a relative configuration with numerous smaller detectors, balancing complexity of electronics, cooling and gaps within the focal plane that would reduce detection coverage; the focal plane design consisting of the two larger detectors was found to be the optimal configuration. (Endicott et al., 2012). The CCDs operate over the 0.2 keV to 5 keV science region of interest range. The radiation sources interact with the spacecraft's mass volume and scatter into secondary particles. Both the primary radiation source particles and secondaries interact with CCDs and induce the instrument background signal. This background source dominates above the intrinsic dark current, readout and system noise of the devices.

Analysis of the instrument background during the design stage of the mission informs on the shielding to be added to the instrumentation. The shielding helps reduce the instrument background in the energy bands for the science regions of interest for the instrumentation to enable science goals to be met. Furthermore, replicating the instrument background through Monte Carlo simulations enables algorithms to be developed to reduce and remove the total number of instrument background events in the images produced from the CCDs. Unless otherwise stated all errors are quoted to a 1-σ significance.

1.1 Radiation Shutter Mechanism

The SMILE SXI instrument includes a Radiation Shutter Mechanism (RSM) which is designed to close a 10 mm thick aluminium shielding door to protect the CCDs when the radiation flux is high. This can occur when entering regions of high radiation levels, such as the Earth's Van Allen radiation belts. The RSM will also close if a solar energetic particle event occurs or if the observatory becomes Sun pointing (Sembay et al., 2016). Therefore, there are two types of closure, the first when travelling below a defined altitude and the second when the radiation intensity increases above a threshold. The RSM door will open again in both circumstances when the spacecraft passes above an altitude threshold. For simplicity, only the altitude closing procedure is included here in the calculation of the unfocussed instrument background.

2 Radiation Environment and Instrument Background

The candidate orbit for SMILE passes through different radiation environments. The environment can be split into two main zones; inside and outside the Van Allen radiation belts. This is also partially used to determine the radiation shutter door position. The radiation shutter door is closed below an altitude threshold that triggers before reaching the Van Allen belts. Radiation environments will be produced for the two door positions.

The radiation environment information was generated using the SPace ENVironment Information System (SPENVIS) tool suite (Heynderickx et al., 2000). Due to orbital precession, the apogee and perigee are perturbed with time. Thus, an averaged fixed "frozen" orbit approximation was used to be representative with inclination set to 73° and apogee and perigee set to 121 000 km and 5000 km respectively . Moreover, the parking and staging orbits are not included in the approximated parameters. This is because the time spent in these orbits is relatively short in comparison to the observational mission time where science operations occur.

Various models in SPENVIS were used to create expected particle fluxes for the mission, for example the AP-8 models for trapped particles and the ISO-15390 model for cosmic ray data. The fluxes used for this work are shown in Figure. 1. The figure includes two Galactic Cosmic Ray (GCR) data sets; solar minima and mission epoch. The former provides the worst-case scenario flux for the GCR source, whilst the latter corresponds to the expected flux of a 2025 launch date. SMILE has a planned 3-year mission lifetime. The particles that form the solar wind attenuate the GCR flux and GCR particles with energy below 1 GeV/n are particularly influenced. Due to this relationship between the solar wind and GCRs, the GCR particles are anti-correlated with the solar cycle. The planned SMILE 2025 launch is near the solar maximum, during this time the GCR flux will be at a minimum. If the Sun is less active during this period, a GCR flux increase might be experienced. Consequently, the spacecraft may observe a higher than predicted instrument radiation background, changes in radiation damage of CCDs or similar effects as the Gaia mission experienced (Crowley et al., 2016; Ahmed et al., 2022).

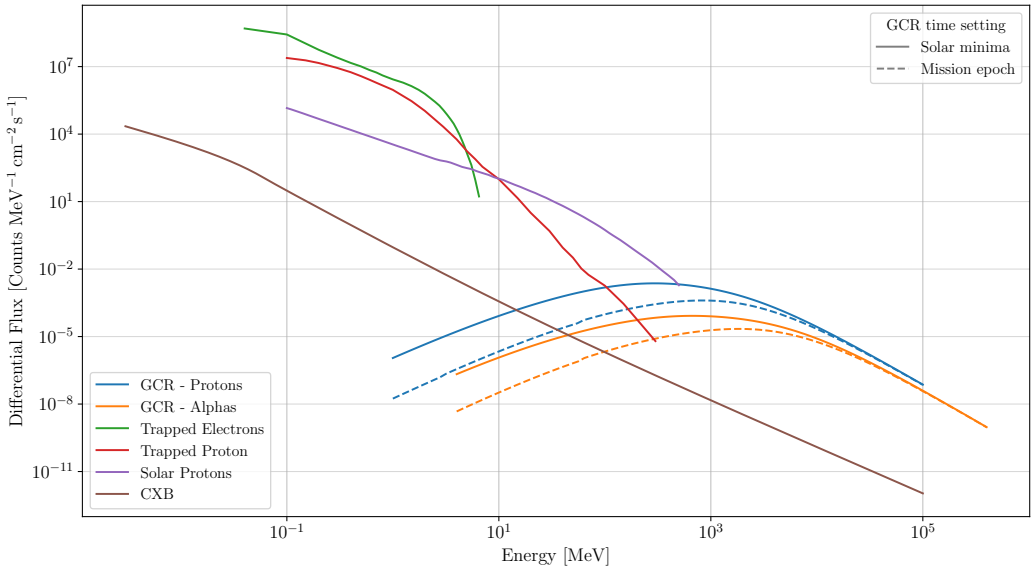

Figure 1: The particle fluxes used in determining the instrument background for the SMILE SXI instrument. Not all sources will be present all the time due to the orbit of the spacecraft.

Due to the planned SMILE launch in 2025, the solar cycle will be near the solar maximum and therefore is more likely to be subject to solar energetic particle events. Solar Energetic Particles (SEPs) are released during these events and are directly linked to the solar activity. Subsequently, there is a greater chance that RSM will be triggered to protect the CCDs at the start of the mission due to an increase in SEPs, reducing observation time. As the mission matures past solar maxima the likelihood of SEP events decreases and therefore the probability of observation times being impacted by RSM closures decreases.

SEPs are partially shielded by the Earth's geomagnetic field, thus, natural shielding is relative to the position along the orbital path. Orbits which are high in altitude or high in latitude are less shielded. SMILE will be more prone to these particle events due to the Highly Elliptical Orbit (HEO). As the SEPs flux is not constant and associated with the solar cycle it is not used in the instrument background calculations and therefore has only been included in the plot for completeness. The SEP instrument background will form part of planned future work into SEP trigger mechanisms.

During the close approach to Earth on the orbital path, the SMILE spacecraft will also enter a radiation environment where albedo particles are present. These albedo particles originate from cosmic rays interacting with the Earth's atmosphere, with the produced secondaries directed towards or away from Earth. The particles directed away from Earth are referred to as splash albedo. It is these particles that will interact with the spacecraft. The splash albedo consists of a hadronic and leptonic component and they both have particle populations that are short-lived and long-lived (Campana et al., 2020). The splash albedo flux decreases with increasing altitudes. As the radiation shutter is closed when passing through this radiation environment and the time in this environment is minimal, the impact to the CCDs will be greatly reduced.

Albedo particles will not contribute to the instrument background as there are no observations during this time along the orbital path. However, they will contribute to

the dose, specifically the neutron albedo that is highest at high latitudes. Therefore, the HEO of SMILE will receive a dose component from these particles but this is expected to be very minor due to both the time spent and the shielding (Ajello et al., 2008; Zhou et al., 2018).

All the particle sources will be present during closed operation. When the radiation shutter door is open, the SMILE spacecraft will be outside the Earth's Van Allen Radiation belts. Therefore, the trapped particle sources will not be present during this operational phase.

These radiation sources contribute to the instrument background. The primaries from these sources interact with the spacecraft structure leading to secondaries, which can deposit energy in the CCDs, causing instrument background. The primary radiations can also directly deposit energy in the CCDs and contribute to the instrument background.

3 Simulation set up

Simulations of the instrument background for the SMILE SXI mission used an internal tool developed in the CEI (Centre for Electronic Imaging) at the OU (The Open University, UK). The tool, the background simulator, is designed to simulate the instrument background for any X-ray based spacecraft given information relating to the geometry and the input radiation source. The geometry information is passed into the software in the form of a Geometry Description Markup Language (GDML) mass model, where volumetric and material definitions are defined. The radiation source is defined in a Geant4 macro file and is created based on the radiation environment for the mission. The particle type, energy range and fluences are included in the macro. The radiation source is generated on a sphere and directional information is sampled from a Lambertian distribution to create a homogeneous isotropic environment around the input mass model.

The background simulator was built using the Geant4 C++ Monte-Carlo toolkit (Allison et al., 2016). The toolkit is responsible for propagating particles through the GDML mass model. The toolkit backend can be tuned via a physics list to match experimental results. The physics list defines the particles, energy limits, physical process models and other properties available at run time for the simulation. Geant4 v10.3.3 and the QBBC physics list form the base of the simulation. Modifications to the physics list included the `G4IonBinaryCascadePhysics` physics processes, auger and Particle-induced X-ray emission (PIXE) atomic de-excitation. The electromagnetic physics list was altered to the Space Users Physics List (SUPL). Developed as part of the ATHENA Radiation Environment Models and X-Ray Background Effects Simulators (AREMBES) study (Dondero & Mantero, 2017), SUPL improves the replication of data between experiments and simulations for use in space. The physics list includes production cuts from 250 eV to 100 TeV and a default cut length of 1 µm. Sensitive detector volumes providing data output for the simulation are assigned based on information located in the mass model. A custom image preprocessor class is attached to the sensitive detector, allowing pixel information to be stored at simulation time rather than being performed during analysis. Grouping of pixels into event clusters is performed during analysis using a nearest neighbour algorithm and the data is processed as unbinned.

Due to the thin CCD (16 µm) active silion volume, a 0.1 µm cut length was set in the sensitive detectors for the SMILE simulations. Two SMILE SXI mass models were used for the simulations, one with the radiation shutter door in an open position and the other in a closed position. The mass models are simplifications of the original Computer-Aided Design (CAD) models that enable radiation transport to occur that is representative of the original CAD. Examples of the mass models are shown in Figure. 2. One

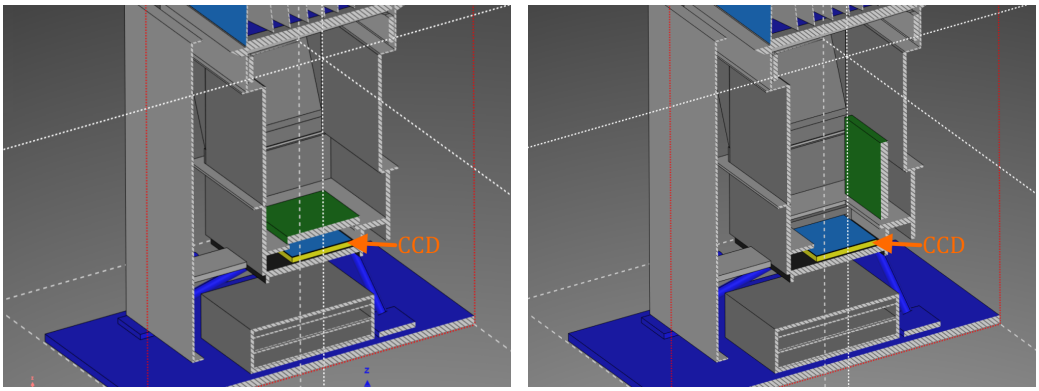

(a) Closed radiation shutter door. (b) Open radiation shutter door.

Figure 2: Open and closed SMILE SXI mass models. The door shown in green moves between the models.

of the main simplifications in the SMILE SXI mass models are the replacement of the Micro Pore Optics (MPOs) with a single slab of material. For high-energy particles, the difference between the MPOs and the slab is minimal, but for low-energy photons, this is not the case. Therefore, these can be simulated separately as a focussed background simulation for any sky component sources. The simulations performed in this paper only relate to the unfocussed component. The number of particles generated per simulation ranged between 10^6 to 10^9 and were dependent on radiation source and mass model.

4 Results and Discussion

4.1 Background rate

The instrument background spectra were simulated for the open and closed models. The two GCR model time settings were also investigated. Both results are shown in Figure. 3. The SMILE red book states that the science Region Of Interest (ROI) is between 0.2 keV to 2.5 keV (Branduardi-Raymont et al., 2018). In this work, a smaller 0.2 keV to 1.4 keV limited analysis band is used. This is due to the background spectrum exhibiting two features that lead to overestimates in the background continuum above 1.4 keV. Both are shown in Figure. 3, the fluorescence lines will be analysed in a later section of this work. Simulations that used hadrons as the incident particle induced fluorescence in the aluminium and silicon in the mass models. These regions are highlighted in the spectra and appear above 1.4 keV. Minimum Ionising Particle (MIP) events are responsible for the sharp rise in the background starting at approximately 2 keV. The energy range in the figure has been extended to include the peak's rise.

The 0.2 keV to 1.4 keV instrument background rates for the spectra in Figure. 3 are presented in Table. 1. Due to the GCR radiation source being anti-correlated with the solar cycle, the GCR flux is higher at solar minimum. The background rate results show this, with GCR solar minima data having higher rates.

Contributions to the instrument background from the GCR - Alpha and CXB sources decrease at both epochs when the radiation shutter door is closed, although this change is not statistically significant for alphas in the mission epoch. The background contribution from the GCR - Proton source decreases with the shutter door closed for solar minimum, but increases during mission epoch. The increase in background rate is due

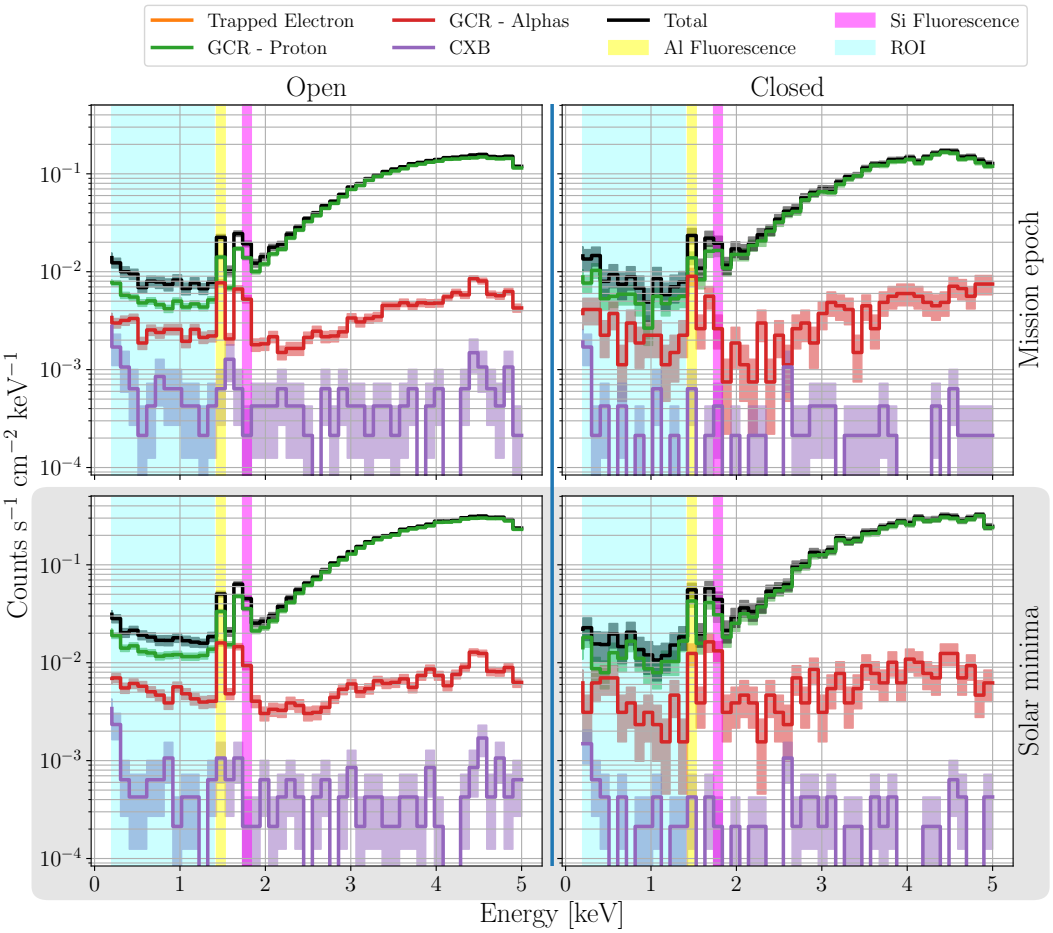

Figure 3: Comparison of the instrument background spectra for different configurations of radiation shutter door position and GCR spectra used. The science 0.2 keV to 1.4 keV region of interest is highlighted in cyan. The two fluorescence lines are shown in yellow and magenta and correspond to the aluminium and silicon Kα lines respectively. Both of the fluorescence lines are outside the region of interest. The silicon Kα appears wider than the aluminium line, this is due to a binning artefact. Trapped electron data is not shown in the energy range in the plots. For the closed data sets trapped electron data starts above $\sim$ 20 keV. Error regions represent a 1 σ error.

to the radiation shutter door acting as a scattering centre for the GCR - Protons. When in the open position, the door is near vertical. Therefore, secondaries generated from the GCR - Protons interacting with the door are less likely to travel towards the plane of the CCDs. The opposite result is observed using the solar minima setting for the GCR - Proton source. The reason for this is the change in the flux rate at different energies. During solar minima, there are more low-energy GCR particles that the radiation shutter door has more of an impact on, reducing their subsequent contribution to the background. It should be noted that the radiation shutter door thickness was chosen independently of these instrument background. For future missions, this instrument background analysis could be performed during early stages to optimise radiation shutter shielding thicknesses.

When the spacecraft is below an altitude threshold, the radiation shutter door closes to protect the instrument from the trapped particle radiation sources. The results in the table show that the contributions to the background from the two trapped sources are zero in the 0.2 keV to 1.4 keV band. These sources do contribute to the background but at energies outside the official 0.2 keV to 2.5 keV band listed in the SMILE red book (Branduardi-Raymont et al., 2018).

Table 1: Instrument background rate for different configurations of radiation shutter door position and GCR spectra used. The background rate is for the 0.2 keV to 1.4 keV region of interest and the units are $\times 10^{-3}$ counts s^{-1} cm^{-2} keV^{-1}. Cells marked with a dash were not simulated and those with just zeros were simulated but produced no data in the region of interest.

Radiation Shutter GCR time setting	Open Mission epoch	Closed Mission epoch	Open Solar minima	Closed Solar minima
GCR - Proton	5.07 ± 0.11	5.84 ± 0.38	12.95 ± 0.30	11.24 ± 0.87
GCR - Alpha	2.51 ± 0.09	2.45 ± 0.28	5.03 ± 0.18	3.84 ± 0.50
CXB	0.67 ± 0.11	0.36 ± 0.08	0.67 ± 0.11	0.38 ± 0.08
Trapped Protons	-	0.0	-	0.0
Trapped Electrons	-	0.0	-	0.0
Total	$\mathbf{8.25 \pm 0.16}$	$\mathbf{8.65 \pm 0.48}$	$\mathbf{18.65 \pm 0.36}$	$\mathbf{15.43 \pm 0.97}$

Table 2: Instrument background rate for the two CCDs. The data shown is from the radiation shutter in the open configurations and the GCR data uses the mission epoch setting. The background rate units are $\times 10^{-3}$ counts s^{-1} cm^{-2} keV^{-1}.

ROI	0.2 keV to 1.4 keV		0.2 keV to 2.5 keV	
CCD370	A	B	A	B
GCR - Proton	5.20 ± 0.16	4.93 ± 0.15	10.48 ± 0.16	10.14 ± 0.16
GCR - Alpha	2.44 ± 0.13	2.59 ± 0.12	2.76 ± 0.10	2.91 ± 0.10
CXB	0.62 ± 0.15	0.72 ± 0.16	0.57 ± 0.10	0.64 ± 0.11
Total	$\mathbf{8.25 \pm 0.16}$	$\mathbf{8.65 \pm 0.48}$	$\mathbf{13.81 \pm 0.20}$	$\mathbf{13.69 \pm 0.21}$

In Table. 1, the total instrument background for the solar minima data is 2.26 times higher than the mission epoch. The mission epoch is currently planned to be near solar maxima. Consequently, the background rate will increase throughout the 3-year mission. The total background rate will be higher during the closed position during the mission epoch. This could cause issues if background field acquisition or other activities such as calibration procedures are performed during this operational period.

Table. 2 lists the simulated SXI instrument background rates for the two CCDs from the open model at the mission epoch. The results in the table show that the rate is within error between the two CCDs. Therefore, any asymmetry in the mass models does not impact the background observed for the two devices. The table also presents the data with the upper limit of the energy band increased to include the two additional spectral features in the background; the fluorescence lines and the MIP peak. For the increased upper band data, the total background increases. Inspection of the individual components reveals that the CXB rate decreases with the energy band upper limit, although this is not statistically significant as it is within 1σ. The additional spectral features are not present in the CXB spectra and are responsible for the increases in the other source components.

The errors in the results presented in the tables and figures include statistical uncertainty from the simulations. The simulated statistical uncertainty is less than 2 % and arises from the Poisson nature of the counting statistics. These statistical errors are propagated through into the final calculations. The systematic errors from the physical models and the simulation physics lists are not included. Work via the AREMBES (ESA, n.d.) study and work by other authors (Basaglia et al., 2016; Batič et al., 2013; Pia et al., 2009; Fioretti et al., 2017; Ivanchenko et al., 2017) aims to address these issues.

4.2 Interaction analysis

Analysis of the previous interaction locations of any detected particle can reveal scattering hotspot regions in the models. Figure. 4 shows a cross-sectional heat map of the last interaction site for all particles incident on the detector. The majority of incident particles originate from structures close to the detector plane. The heat maps also show that the radiation shutter door is a region where many detected particles originate.

Views of the previous interaction locations of detected particles from the two SXI CCDs are shown in Figure. 5 for the GCR - Proton source of the open model. The heat maps indicate a bias in the interaction locations regions due to the position of the detectors. Due to the asymmetrical location of the Electronics Box (EBox), CCD370 B detects a higher amount of scattered particles from this mass volume than CCD370 A. The background rates have already shown that there is no asymmetry in the rates with the current simulations to a 2 % statistical significance. If other external masses with asymmetrical locations are included in future simulations, asymmetry in the background rates might be observed.

4.3 Fluorescence analysis

The background spectra plots shown in the prior sections have included the fluorescence lines highlighted. The flux of the fluorescence lines are measured to determine if different configurations of the simulations cause more or less fluorescence. The fluorescence line fluxes have had the background continuum subtracted and associated errors incorporated in the error analysis. The flux of the aluminium K_α line for the open and closed model are compared in Table. 3. Due to particles scattering from the radiation shutter door, the aluminium fluorescence is higher for the closed model. The radiation shutter door in a closed position fills the entire field of view of the detector, which is the source of the aluminium fluorescence. In the open position, the door only fills a small portion of the field of view and is further from the CCDs by comparison. The origins for the aluminium fluorescence for the open and closed configurations are shown in Figures. 6a and 6b. The radiation shutter door is observed face-on in the open position data set.

When at the mission epoch, the majority of the induced aluminium fluorescence is shared between the two GCR sources. For the solar minima data, the same split is observed when the door is open. However, when the door is closed, the GCR - Protons become the dominant cause of fluorescence. This is related to the shutter door being a scattering and fluorescence centre and the solar minima flux containing more low-energy particles aiding in fluorescence.

Table. 4 lists the silicon K_α fluorescence line flux for the different simulation configurations. Unlike the aluminium fluorescence that increases when the radiation shutter door closes, the silicon fluorescence decreases. This is because the door reduces the number of particles interacting with the detector package where fluorescing silicon is located. This is confirmed in Figures. 6c and 6d that shows the origin of the silicon fluorescence. The majority of the silicon is the support wafer. Therefore, thinning this re-

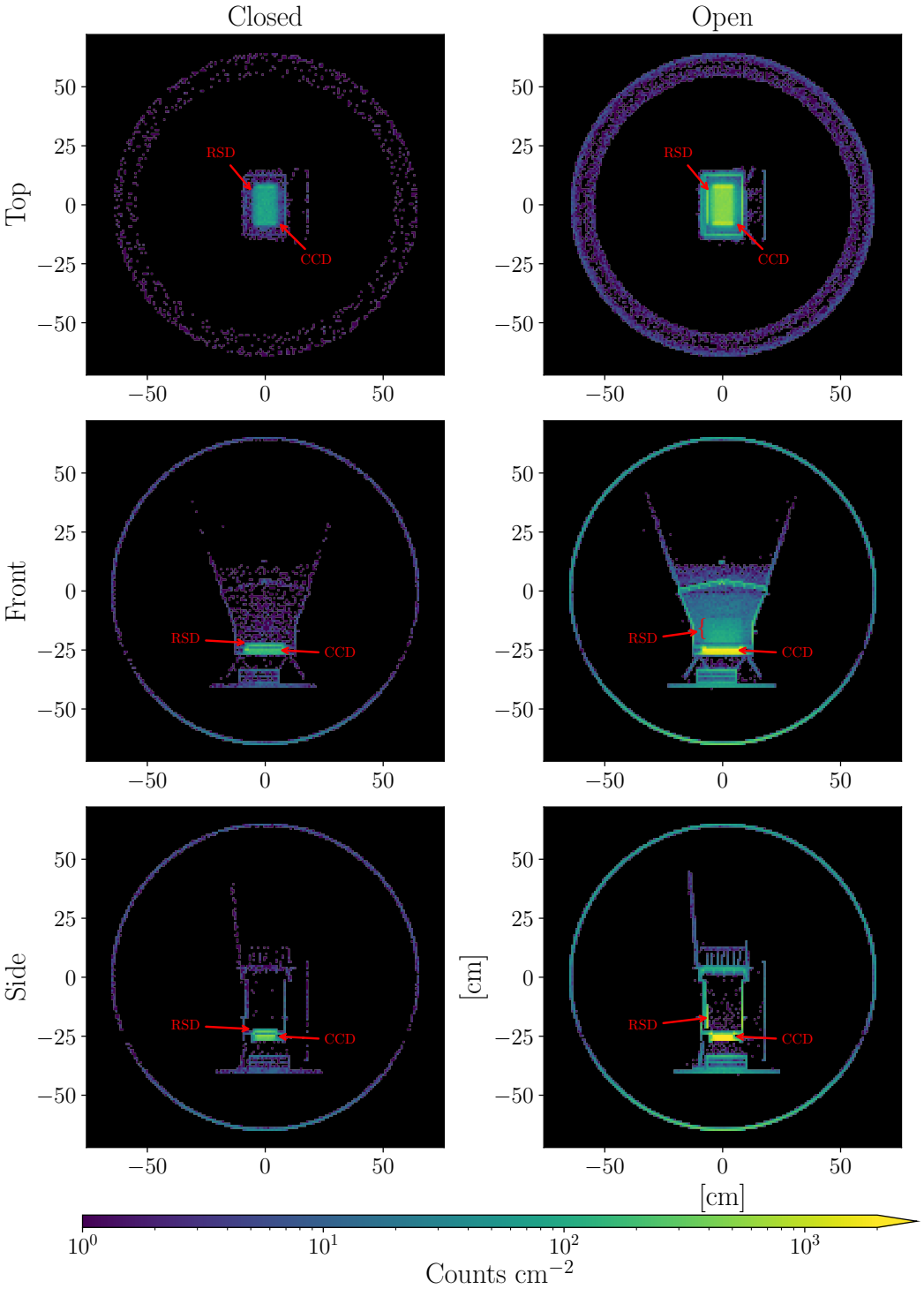

Figure 4: Comparison of interaction location heat maps between the open and closed models. The heat maps show the locations of the last interaction for particles which hit the detector. The visible outer ring is a section of the sphere on which primary particles are generated. The histograms represent 10 cm slices through the mass model and the colour intensity is logarithmic. The data set used to create the histograms uses the GCR particle sources using the mission epoch setting. The CCD and Radiation Shutter Door (RSD) are labelled. The top configuration displays a thicker outer ring, this is due to a larger cross section chosen to capture the radiation shutter door.

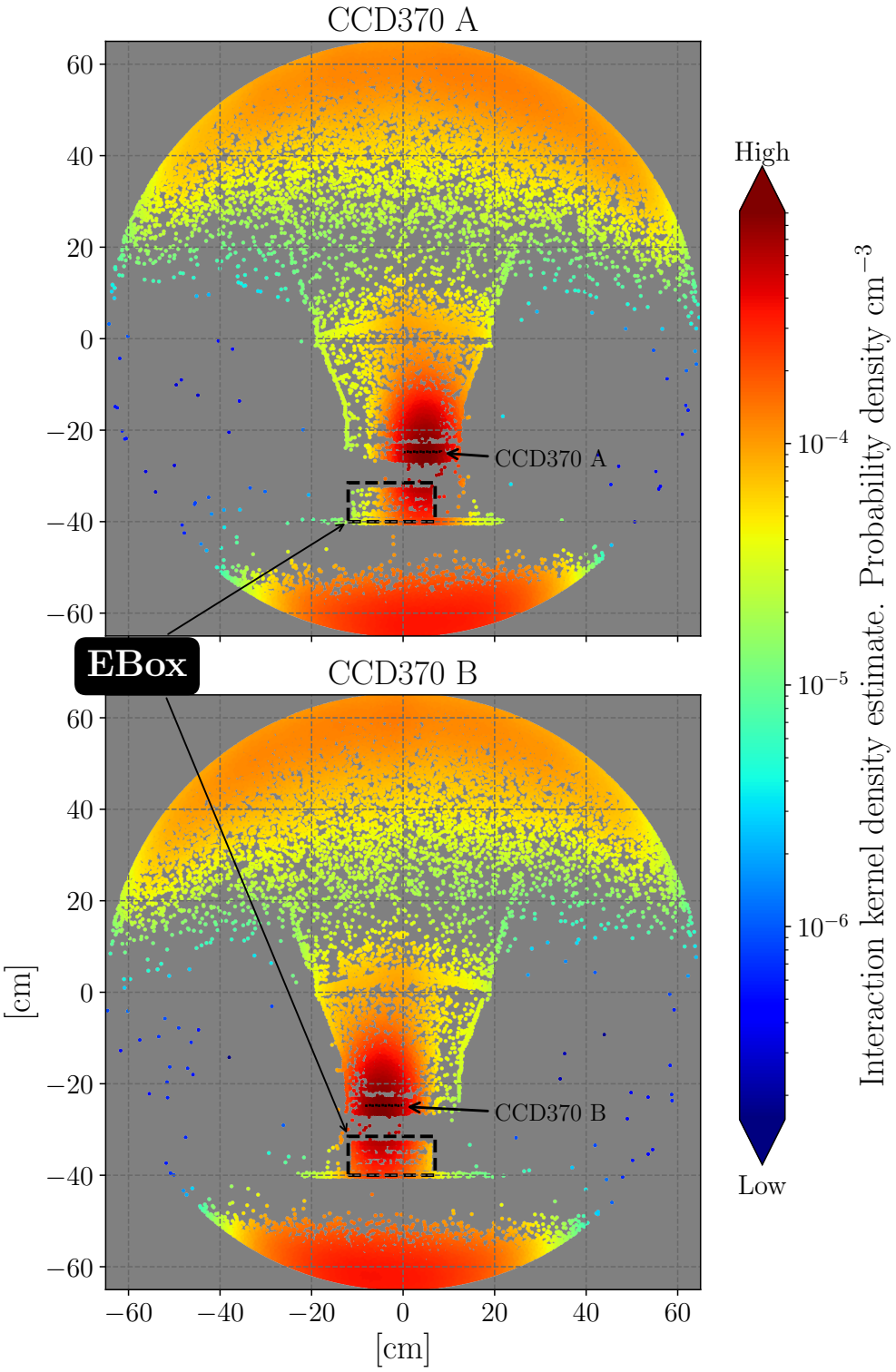

Figure 5: Comparison of the instrument background spectra previous interaction locations for the two CCDs in the energy region of 0 keV to 5 keV. The data shown is for the open model with the mission epoch time setting for the GCR source. The data shown are only from the GCR - Proton source. The colour scale is based on the output of a Gaussian kernel density estimator applied to the location data.

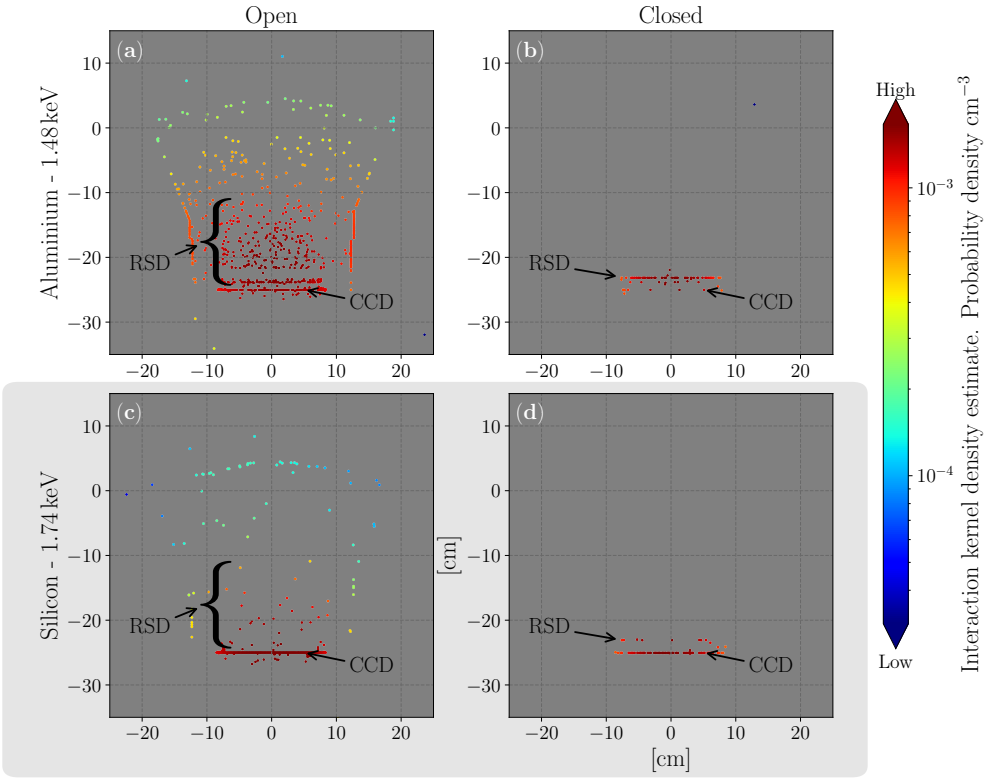

Figure 6: Origin of fluorescence line energies. The kernel density histograms show the location of the previous interaction location before being detected. A Gaussian kernel density estimator has been applied to generate the colours, which corresponds to density of the interaction locations. Some points shown will be caused by scattering rather than a fluorescence physics process. The data sets use the GCR spectra with the mission epoch setting. The plots show contributions from all sources i.e. GCR, CXB and trapped particles for the closed models. The CCD and Radiation Shutter Door (RSD) are labelled.

Table 3: Aluminium K_α (1.486 keV) fluorescence line flux ($\times 10^{-3}\,cm^{-2}\,s^{-1}$).

Radiation Shutter GCR time setting	Open Mission epoch	Closed Mission epoch	Open Solar minima	Closed Solar minima
GCR - Proton	0.57 ± 0.51	0.45 ± 0.55	1.10 ± 1.44	2.23 ± 1.30
GCR - Alphas	0.45 ± 0.20	0.65 ± 0.24	0.93 ± 0.42	0.57 ± 0.67
CXB	0.06 ± 0.06	0.05 ± 0.04	0.06 ± 0.06	0.03 ± 0.03
Trapped Proton	-	0.00	-	0.00
Trapped Electron	-	0.00	-	0.00
Total	$\mathbf{1.08 \pm 0.73}$	$\mathbf{1.15 \pm 0.77}$	$\mathbf{2.08 \pm 1.88}$	$\mathbf{2.83 \pm 1.98}$

gion could reduce the silicon fluorescence at the expense of lowering shielding close to the CCDs.

5 Discussion

The SMILE mission is planned to launch into a highly elliptical Earth orbit. During the orbit, it will pass through multiple radiation environments. The SMILE SXI instrument includes a radiation shutter door that closes to reduce the number of particles

Table 4: Silicon K_α (1.740 keV) fluorescence line flux ($\times 10^{-3}\,\mathrm{cm^{-2}\,s^{-1}}$).

Radiation Shutter GCR time setting	Open Mission epoch	Closed Mission epoch	Open Solar minima	Closed Solar minima
GCR - Proton	0.64 ± 0.36	0.49 ± 0.43	2.62 ± 0.71	1.64 ± 1.14
GCR - Alphas	0.41 ± 0.23	0.27 ± 0.32	0.89 ± 0.48	1.16 ± 0.51
CXB	0.03 ± 0.05	0.01 ± 0.03	0.05 ± 0.06	0.03 ± 0.03
Trapped Proton	-	0.00	-	0.00
Trapped Electron	-	0.00	-	0.00
Total	$\mathbf{1.08 \pm 0.53}$	$\mathbf{0.77 \pm 0.65}$	$\mathbf{3.56 \pm 1.13}$	$\mathbf{2.83 \pm 1.65}$

interacting with the CCDs. This helps reduce dose damage and reduce instrument background. During closed portions of the orbit, the CCDs will not be able to perform science operations. Therefore, the instrument background during the open periods of operation is important to analyse. The SMILE SXI instrument includes micro pore optics in a lobster eye optic configuration. Some of the radiation will be focussed through the optics increasing the instrument background. This work does not include the focussed contribution as it is being studied in a separate body of work. Simulations were performed for the unfocussed instrument background across a variety of scenarios including solar minima and solar maxima.

The simulations found that the majority of the unfocussed instrument background arises from the GCR sources, which are anti-correlated with the solar cycle. The current expected launch date for SMILE is 2025 which is close to solar maxima. Therefore, the flux of the GCR source will increase with mission duration. The unfocussed instrument background rate was estimated to be $(8.25 \pm 0.16) \times 10^{-3}\,\mathrm{counts\,s^{-1}\,cm^{-2}\,keV^{-1}}$ during solar maxima. The instrument background was also evaluated at solar minima and determined to be $(1.865 \pm 0.036) \times 10^{-2}\,\mathrm{counts\,s^{-1}\,cm^{-2}\,keV^{-1}}$ when the radiation shutter door is open. This is $\times 2.25$ higher than when at solar maxima near mission epoch. Therefore, the instrument background rate will also increase with mission duration due to the GCR component of the radiation background.

Analysis of previous particle interaction locations before detection was performed for the two CCDs that form the SMILE SXI focal plane array (FPA). The results showed some asymmetry in background origins for the two devices. The placement of the electronics box is off centre and leads to the small asymmetry. CCD370 B detects more background that scatters off of this external mass. The background rates for the two CCDs were similar within error and showed no statistical differences. For future missions that use multiple detectors, it is important to be aware of additional asymmetrically placed external masses, as they could make background rates differ between the detectors.

The closed configuration was also explored and revealed a higher instrument background of $(8.65 \pm 0.48) \times 10^{-3}\,\mathrm{counts\,s^{-1}\,cm^{-2}\,keV^{-1}}$. Although not statistically significant in comparison to the open data set, this higher value for the closed data is due to the radiation shutter covering more of the detection field of view when in the closed position. The particles subsequently scatter off the shutter door into the detector resulting in higher background. The aluminium fluorescence increases with the portion of the radiation shutter door filling the detector field of view. Therefore, careful consideration is advised if operations such as the collection of dark frames are planned during shutter closure.

Due to the importance of X-ray background simulations as previously mentioned, these simulations are even more important when considering that the science goals of SMILE SXI are the study of the interaction between the solar wind and the Earth's magnetosphere and ionosphere. The SXI telescope will detect X-rays produced by the so-

lar wind charge exchange (SWCX) mechanism, caused by the interaction of solar wind ions with neutral atoms within the Earth's magnetosphere. The SXI images will be used to identify the magnetospheric nose and cusps and detect the magnetopause boundary. Magnetohydrodynamic models have been extensively used to simulate the SWCX emission under different solar wind and interplanetary magnetic field conditions (e.g. (Whittaker et al., 2016)). These simulations, as well as actual observations of the SWCX emission from other X-ray missions such as XMM (Carter et al., 2011) have been used to estimate the expected SWCX X-ray signal measured by the SXI.

The other signal components present in SXI images are the astrophysical X-ray sources in the Field-of-View, the diffuse soft X-ray background (SXBG, whose intensity for the SXI can be estimated for example from its measurement by the ROSAT mission all-sky maps), the instrumental background, modelled and presented in this paper, and the Manganese and Aluminium K-alpha emission lines from the on-board radioactive sources, used for calibration purposes.

In the main SXI science band, below 1.5 keV, the SWCX intensity will be the strongest signal measured by the SXI for high solar wind fluxes. The main component of the background is the diffuse SXBG, while the signal from the particle-induced background, as estimated in this work, is negligible, more than an order of magnitude fainter. Conversely, for the low solar wind case the charge exchange signal can actually be fainter than the extra-galactic diffuse background, but still well above the instrumental background at soft energies.

The particle-generated background only starts to dominate at energies above $\sim 2\,\mathrm{keV}$, and therefore can have a significant impact on the SXI secondary science, constituted of astrophysical point and diffuse X-ray sources. For example, the strong instrument background at high energies will affect the detection and the measurement of very absorbed sources such as Compton-thick AGNs.

6 Summary

The unfocussed instrument background for SMILE SXI has been estimated to be $(8.25 \pm 0.16) \times 10^{-3}\,\mathrm{counts\,s^{-1}\,cm^{-2}\,keV^{-1}}$ at mission epoch near solar maxima when the radiation shutter door is open. Through out the mission lifetime, the unfocussed background will increase due to the anti-correlation of the GCR sources with the solar cycle. The GCR sources contribute over 90 % of the instrument background. A maximum unfocussed background will occur at solar minimum with an estimate of $(1.865 \pm 0.036) \times 10^{-2}\,\mathrm{counts\,s^{-1}\,cm^{-2}\,keV^{-1}}$, this will only occur if the mission is extended to a 5.5 year mission from a 3 year mission.

During operation with the radiation shutter door closed, the unfocussed instrument background can be higher due to particles scattering off of the door directly into the detector's field of view. During mission epoch the closed background was estimated to be $(8.65 \pm 4.80) \times 10^{-3}\,\mathrm{counts\,s^{-1}\,cm^{-2}\,keV^{-1}}$, which could pose an issue if the CCDs are planned to perform background estimates or collect frames for background subtraction during this period.

Acknowledgments

This work was supported by the following grants: SMILE 2019–2022 STFC (Grant reference: ST/T003138/1); SMILE 2022–2023 ESA (Contract No: 4000138219/22/NL/BW/pbe).

References

Ahmed, S., Hall, D. J., Crowley, C. M., Skottfelt, J. M., Dryer, B., Seabroke, G., ...

Holland, A. D. (2022). Understanding the evolution of radiation damage on the Gaia CCDs after 72 months at L2. *Journal of Astronomical Telescopes, Instruments, and Systems*, *8*(1), 016003. Retrieved from `https://doi.org/10.1117/1.JATIS.8.1.016003` doi: 10.1117/1.JATIS.8.1.016003

Ajello, M., Greiner, J., Sato, G., Willis, D., Kanbach, G., Strong, A., ... others (2008). Cosmic x-ray background and earth albedo spectra with swift bat. *The Astrophysical Journal*, *689*(2), 666.

Allison, J., et al. (2016). Recent developments in geant4. *Nuclear Instruments and Methods in Physics Research Section A: Accelerators, Spectrometers, Detectors and Associated Equipment*, *835*, 186 - 225. Retrieved from `http://www.sciencedirect.com/science/article/pii/S0168900216306957` doi: https://doi.org/10.1016/j.nima.2016.06.125

Basaglia, T., Han, M. C., Hoff, G., Kim, C. H., Kim, S. H., Pia, M. G., & Saracco, P. (2016). Quantitative test of the evolution of geant4 electron backscattering simulation. *IEEE Transactions on Nuclear Science*, *63*(6), 2849-2865.

Batič, M., Hoff, G., Pia, M. G., Saracco, P., & Weidenspointner, G. (2013). Validation of geant4 simulation of electron energy deposition. *IEEE Transactions on Nuclear Science*, *60*(4), 2934-2957.

Branduardi-Raymont, G., Wang, C., Escoubet, C., Adamovic, M., Agnolon, D., Berthomier, M., ... others (2018). *Smile definition study report (red book).*

Campana, R., Fuschino, F., Labanti, C., Mereghetti, S., Virgilli, E., Fioretti, V., ... Amati, L. (2020). The xgis instrument on-board theseus: Monte carlo simulations for response, background, and sensitivity. In *Space telescopes and instrumentation 2020: Ultraviolet to gamma ray* (Vol. 11444, pp. 1245–1253).

Carter, J., Sembay, S., & Read, A. (2011). Identifying XMM-Newton observations affected by solar wind charge exchange–Part II. *Astronomy & Astrophysics*, *527*, A115.

Crowley, C., Abreu, A., Kohley, R., Prod'homme, T., & Beaufort, T. (2016). Radiation effects on the gaia ccds after 30 months at l2. In *High energy, optical, and infrared detectors for astronomy vii* (Vol. 9915, pp. 204–218).

Dondero, P., & Mantero, A. (2017). *A 'space dedicated' physics list from the arembes project.* Retrieved from `https://indico.esa.int/event/160/contributions/1136/contribution.pdf` (12th Geant4 Space User Workshop)

Endicott, J., Walker, A., Bowring, S., Turner, P., Allen, D., Piersanti, O., ... Walton, D. (2012). Charge-coupled devices for the esa plato m-class mission. In *High energy, optical, and infrared detectors for astronomy v* (Vol. 8453, pp. 466–472).

ESA. (n.d.). *Athena radiation environment models and x-ray background effects simulators.*

Fioretti, V., Bulgarelli, A., Malaguti, G., Bianchin, V., Trifoglio, M., & Gianotti, F. (2012). The low Earth orbit radiation environment and its impact on the prompt background of hard x-ray focusing telescopes. In A. D. Holland & J. W. Beletic (Eds.), *High energy, optical, and infrared detectors for astronomy v* (Vol. 8453, p. 845331). SPIE. Retrieved from `https://doi.org/10.1117/12.926248` doi: 10.1117/12.926248

Fioretti, V., Mineo, T., Bulgaerilli, A., Dondero, P., Ivanchenko, V., Lei, F., & Lotti, S. (2017). Geant4 simulations of soft proton scattering in x-ray optics. *Exp Astron*, *44*, 413-435.

Heynderickx, D., Quaghebeur, B., Speelman, E., & Daly, E. (2000). Esa's space environment information system (spenvis)-a www interface to models of the space environment and its effects. In *38th aerospace sciences meeting and exhibit* (p. 371).

Ivanchenko, V., Dondero, P., Fioretti, V., Ivantchenko, A., Lei, F., Lotti, S., & Mantero, A. (2017). Geant4 simulations of soft proton scattering in x-ray optics.

Exp Astron, *44*, 437-450.

Pia, M. G., Weidenspointner, G., Augelli, M., Quintieri, L., Saracco, P., Sudhakar, M., & Zoglauer, A. (2009). Pixe simulation with geant4. *IEEE Transactions on Nuclear Science*, *56*(6), 3614-3649.

Raab, W., Branduardi-Raymont, G., Wang, C., Dai, L., Donovan, E., Enno, G., ... others (2016). Smile: A joint esa/cas mission to investigate the interaction between the solar wind and earth's magnetosphere. In *Space telescopes and instrumentation 2016: Ultraviolet to gamma ray* (Vol. 9905, p. 990502).

Sembay, S., Branduardi-Raymont, G., Drumm, P., Escoubet, C. P., Genov, G., Gow, J., ... others (2016). The soft X-ray imager (SXI) on the SMILE Mission. In *Agu fall meeting abstracts* (pp. SM44A–04).

Soman, M., Hall, D., Holland, A., Burgon, R., Buggey, T., Skottfelt, J., ... others (2018). The smile soft x-ray imager (sxi) ccd design and development. *Journal of Instrumentation*, *13*(01), C01022.

Whittaker, I. C., Sembay, S., Carter, J. A., Read, A. M., Milan, S. E., & Palmroth, M. (2016). Modeling the magnetospheric X-ray emission from solar wind charge exchange with verification from XMM-Newton observations. *Journal of Geophysical Research: Space Physics*, *121*(5), 4158–4179.

Zhou, D., Sun, Y., Zhang, B., Zhang, S., Sun, Y., Liang, J., ... others (2018). Radiation measured for chinese satellite sj-10 space mission. *Journal of geophysical research: space physics*, *123*(2), 1690–1700.